SANDIA REPORT
SAND2006-0390
Unlimited Release
Printed February 2006

Quantum Coherence in Semiconductor Nanostructures for Improved Lasers and Detectors LDRD Final Report

Jeffrey G. Cederberg, Weng W. Chow, Normand A. Modine, S. Ken Lyo,
and Robert M. Biefeld

Prepared by
Sandia National Laboratories
Albuquerque, New Mexico 87185 and Livermore, California 94550

Sandia is a multiprogram laboratory operated by Sandia Corporation,
a Lockheed Martin Company, for the United States Department of Energy's
National Nuclear Security Administration under Contract DE-AC04-94AL85000.

Issued by Sandia National Laboratories, operated for the United States Department of Energy by Sandia Corporation.

Available to DOE and DOE contractors from
U.S. Department of Energy
Office of Scientific and Technical Information
P.O. Box 62
Oak Ridge, TN 37831

Telephone: (865) 576-8401
Facsimile: (865) 576-5728
E-Mail: reports@adonis.osti.gov
Online ordering: http://www.osti.gov/bridge

Available to the public from U.S. Department of Commerce
National Technical Information Service
5285 Port Royal Rd.
Springfield, VA 22161

Telephone: (800) 553-6847
Facsimile: (703) 605-6900
E-Mail: orders@ntis.fedworld.gov
Online order: http://www.ntis.gov/help/ordermethods.asp?loc=7-4-0#online

SAND 2006-0390
Unlimited Release
Printed February 2006

Quantum Coherence in Semiconductor Nanostructures for Improved Lasers and Detectors

Jeffrey G. Cederberg and Robert M. Biefeld
Advanced Material Sciences Department

Weng W. Chow and S. Ken Lyo
Semiconductor Material and Device Sciences

Normand A. Modine
Nanostructure and Semiconductor Physics

Sandia National Laboratories
P.O. Box 5800
Albuquerque, NM 87185

Abstract

The potential for implementing quantum coherence in semiconductor self-assembled quantum dots has been investigated theoretically and experimentally. Theoretical modeling suggests that coherent dynamics should be possible in self-assembled quantum dots. Our experimental efforts have optimized InGaAs and InAs self-assembled quantum dots on GaAs for demonstrating coherent phenomena. Optical investigations have indicated the appropriate geometries for observing quantum coherence and the type of experiments for observing quantum coherence have been outlined. The optical investigation targeted electromagnetically induced transparency (EIT) in order to demonstrate an all optical delay line.

CONTENTS

1.0 INTRODUCTION

The goal of the LDRD has been the observation of quantum coherence (QC) effects in self-assembled quantum dots (SAQD). Quantum coherence effects are a broad class of phenomena that occur when the excess carriers generated in a material retain their initial phase long enough to interact with other carriers coherently. The phenomena include lasing without inversion, electromagnetically induced transparency (EIT), and dark state spectroscopy. Technologically this could result in the demonstration of an all-optical delay or an optical quantum bit, or qubit, in semiconductors SAQD. SAQD are possibly better than quantum wells for this observation because the coherence lifetimes are longer. The homogeneous lifetime, the time constant for phase retention in SAQD has been measured to be 250 femtoseconds at room temperature [1]. This contrasts to 30 to 70 femtoseconds for homogeneous lifetimes in quantum wells. This lifetime increases significantly at low temperatures for SAQD to 600 to 800 picoseconds at liquid helium temperatures [2, 3]. Our efforts have concentrated on developing the theory which establishes the conditions for observation of optical coherence effects, preparing SAQD samples, and identifying conditions optimal for experimental observation of quantum coherence effects in semiconductors and the types of experiments needed. The results from each of these efforts will be described below.

2.0 QUANTUM COHERENCE THEORETICAL DEVELOPMENTS

A theory of quantum coherence and interference was developed for a semiconductor system. This theory predicts LWI, EIT and refractive index enhancement in the transient regime, even for dephasing rates typical under room temperature and high excitation conditions. It also indicates important deviations from atomic systems, because of a strong influence of the continuum comprised of states from the surrounding quantum well. The dot-well Coulomb coupling gives rise to collision-induced population redistribution and many-body energy and field renormalizations. Together, they modify the magnitude, spectral shape and time

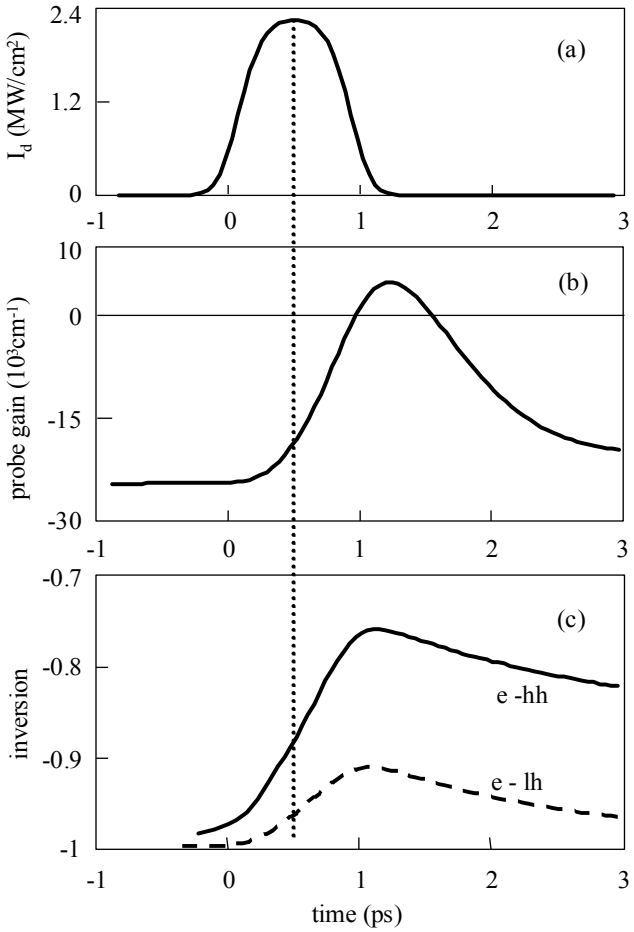

Figure 1. (a) Drive pulse, (b) probe signal absorption or gain, and (c) inversion in electron to heavy (solid curve) and light (dashed curve) transition versus time. Gain is observed without inverting either transition.

dependence of quantum interference. Figures 1 (a) and (b) show the temporal relationship between drive pulse and optical response to weak probe signal. At the probe frequency, there is an abrupt bleaching of the absorption after the onset of the drive pulse. This is followed by the appearance of gain for a very short duration, after which absorption reappears, but at a smaller value than prior to the drive pulse. Figure 1 (c) indicates that while the drive pulse creates an inversion in, there is no inversion on the probe signal, even when the probe signal experiences optical gain. Carrier density (created by the drive pulse) at the gain maximum is 1.35×10^{10} cm^{-3} which is an order of magnitude lower than the 1×10^{11} cm^{-2} necessary to obtain transparency in the absence of LWI.

3.0 SELF-ASSEMBLED QUANTUM DOT GROWTH STUDIES

Previous research on epitaxial growth of SAQD had enabled demonstrations of InGaAs SAQD heterostructures in the GaAs/AlGaAs system. This potential coupled with the long homogeneous lifetimes observed for SAQD suggested this as a possible system for experimentation. The desire early in this LDRD was to develop SAQD that would have optical transitions in the visible or near infrared (emission less than 1 μm) to utilize the optical equipment (sources and detectors) at these wavelengths. Our efforts on this system are summarized in Section 3.1. Initial growth efforts demonstrated $In_{0.4}Ga_{0.6}As$ SAQD with room temperature emission at 1075 nm. The problem with these structures is that the inhomogeneous lifetime is as small as 165 femtoseconds (80 meV). The other disadvantage with these structures is that there was no clear excited state observed at room temperature to form the three energy level system needed to observe QC effects. This cooled interest in $In_{0.4}Ga_{0.6}As$ SAQD and led to efforts to improve the inhomogeneous lifetime of InAs SAQD. Longer lifetimes of 290 femtoseconds (45 meV) were obtained with clear excited state resonances at room temperature. This was selected as the target system for further nonlinear optical investigations. Section 3.2 summarizes the growth investigations in binary InAs SAQD.

3.1 Growth investigations on InGaAs alloy SAQD

The two-dimensional to three-dimensional transformation of compressively strained epitaxial layers has been identified as a route to self-assembled nanostructures. This transformation occurs for a large number of semiconductor systems and has been investigated extensively in an attempt to optimize this process to form self-assembled nanostructures [4,5]. InGaAs on GaAs(001) is one such system that has optoelectronic applications[6,7]. We have investigated the growth of $In_{0.4}Ga_{0.6}As$ on GaAs by metal-organic vapor phase epitaxy (MOVPE)

to form self-assembled quantum dots (SAQD) with a band gap greater than 1.24 eV (1.0 μm). Many investigations have discussed the mechanisms associated with self-assembled quantum dot formation. There is an ongoing debate about the role of thermodynamics relative to kinetics during the islanding process. My investigations propose that thermodynamics in the form of surface segregation plays a role. If surface segregation can be controlled, the three-dimensional transformation can be eliminated to extend planar growth for highly strained films or enhanced to form uniform dense SAQD with a minimum wetting layer.

Surface segregation occurs during the growth of alloys when one of the components is rejected from the bulk resulting in a surface phase that is enriched relative to the bulk composition. The surface phase in the case presented here is an alloy with a different composition from the bulk. The surface segregation of In during InGaAs growth on GaAs growth is well documented [8,9,10]. It limits the growth of abrupt quantum wells and introduces interface scattering in channels of InGaAs/AlGaAs high electron mobility devices [11,12]. For InAs deposition on GaAs, segregation of In to the surface has been observed using *in situ* surface science tools and strain sensitive techniques. Measurement of the strain induced curvature of thin substrates suggests an amorphous or adsorbed layer exists on the surface [13]. These results are consistent with thermodynamic analysis of highly strained heteroepitaxy, which predicts an amorphous layer [14]. Angle resolved x-ray photoemission spectroscopy and auger electron spectroscopy have estimated the thickness of the segregated layer to be several monolayers [8] and reflection high energy electron diffraction has been use to estimate the surface composition from the two-dimensional to three-dimensional transition [15].

My investigations confirm previous results that growth condition can suppress or enhance three-dimensional growth. This investigation examines the growth of $In_{0.4}Ga_{0.6}As$ under

different AsH_3 partial pressures and different growth temperatures. Lower growth temperatures have been identified previously as reducing surface segregation [11,12], but the role of AsH_3 on QD formation has only been speculated [16,17]. Conditions where surface segregation is suppressed and enhanced are identified. This work casts these observations and the present results in terms of surface segregation allowing interpretation of different growth conditions and prediction of conditions that will limit or enhance QD formation. The results are explained in terms of modifications to the thickness of the segregated layer on the surface.

3.1.1 Experimental Details

$In_{0.4}Ga_{0.6}As$ was deposited using low pressure MOVPE operating at 70 torr in a high speed (900 rpm) rotating disk chamber. Triethyl gallium (TEGa) and trimethyl indium (TMIn) both held at 850 mbar and 20°C were the group III metal-organics used and arsine (AsH_3) was group V hydride utilized. GaAs (001) ± 0.1° substrates were heated to 650°C, annealed in AsH_3 for 5 minutes to desorb the surface oxide, and followed up with a 100 nm GaAs buffer. After cooling to 600°C a 200 nm GaAs buffer was then grown. The sample was then cooled under AsH_3 to the temperature desired for $In_{0.4}Ga_{0.6}As$ growth, which was deposited under varied conditions. The growth rate of $In_{0.4}Ga_{0.6}As$ was held constant in these studies at 0.2 nm/second. After deposition of the $In_{0.4}Ga_{0.6}As$ the chamber was purged for 10 seconds under hydrogen to remove AsH_3 and metal-organics. After the hydrogen purge, the $In_{0.4}Ga_{0.6}As$ layer was capped with 3 nm of GaAs grown at the $In_{0.4}Ga_{0.6}As$ growth temperature. The capped sample was heated to 600°C for growth of 300 nm of GaAs. The sample was subsequently cooled for growth of uncapped $In_{0.4}Ga_{0.6}As$ under the same conditions that were used for the buried layer. Photoluminescence (PL) and atomic force microscopy (AFM) were performed on the same sample. The InGaAs growth rate and composition were calibrated using high resolution x-ray

diffraction from InGaAs/GaAs superlattices around the (004) and (224) reflections, analyzing the results to account for relaxation during growth [18,19].

PL was performed at room temperature using an Accent RPM2000 photoluminescence mapping system using 785 nm laser with a power density of 4.5 W/cm^2 and detected through a 530 nm high pass filter with an InGaAs detector. AFM was performed in air at room temperature using a Digital Instruments Nanoscope III with silicon tips, with an approximately 5 nm radius, using tapping mode.

3.1.2 Results

The morphology of InGaAs films varies dramatically as the growth temperature is changed as depicted in Figure 2. At low growth temperatures (Figure 2a, 450°C) the morphology is dominated by a low density (46 μm^{-2}) of small elliptically shaped islands. The islands range from 30 by 20 nm to 45 by 30 nm in lateral size, with heights of 4 ± 2 nm. As the

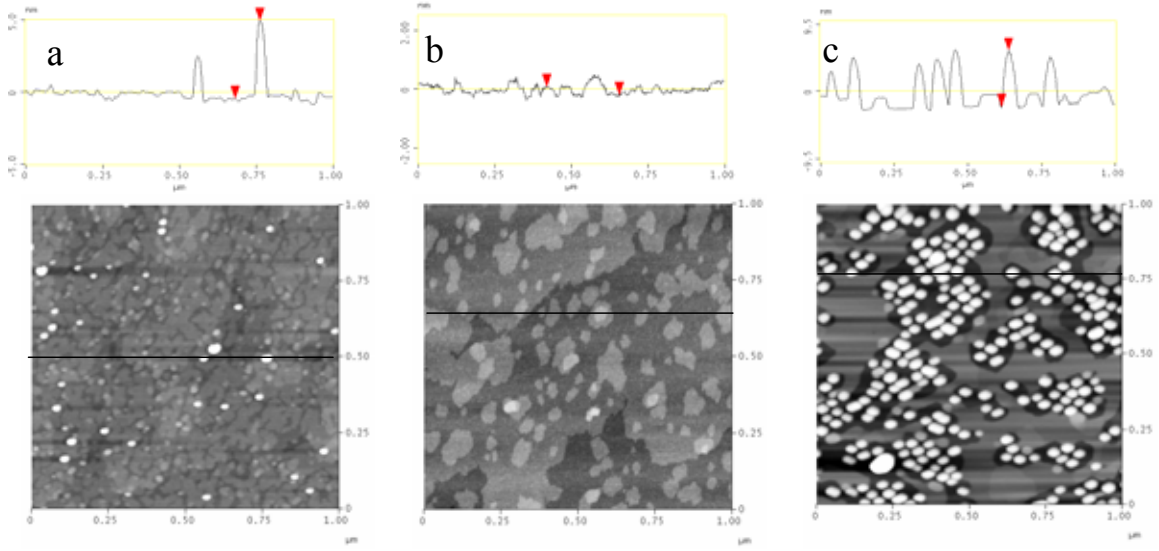

Figure 2. AFM images of InGaAs surfaces as a function of temperature for high AsH_3 partial pressure. The temperatures used are a) 450°C, b) 500°C, c) 550°C. The inlet AsH_3 partial pressure was maintained at 0.27 torr and the thickness deposited was 4.5 nm for all the samples. Top sections showing topography correspond to the horizontal line in each image. The vertical image scales are 10, 5, and 20 nm, respectively.

temperature is increased (Figure 2b, 500°C) the density of three-dimensional islands drops to near zero. Only small two-dimensional, monolayer islands are observed with a density of approximately 100 μm^{-2}. As the temperature is increased further (Figure 2c, 550°C) the density of larger three-dimensional islands increases dramatically to over 200 μm^{-2}, forming patches of islands, isolated by bare surface. The lateral extent of the islands ranges from 40 × 30 nm to 50 by 30 nm. The island height is 5 ± 1 nm.

The observed discontinuity in the island formation is difficult to understand unless other parameters beside the growth temperature are considered. Figure 3 shows the effect of

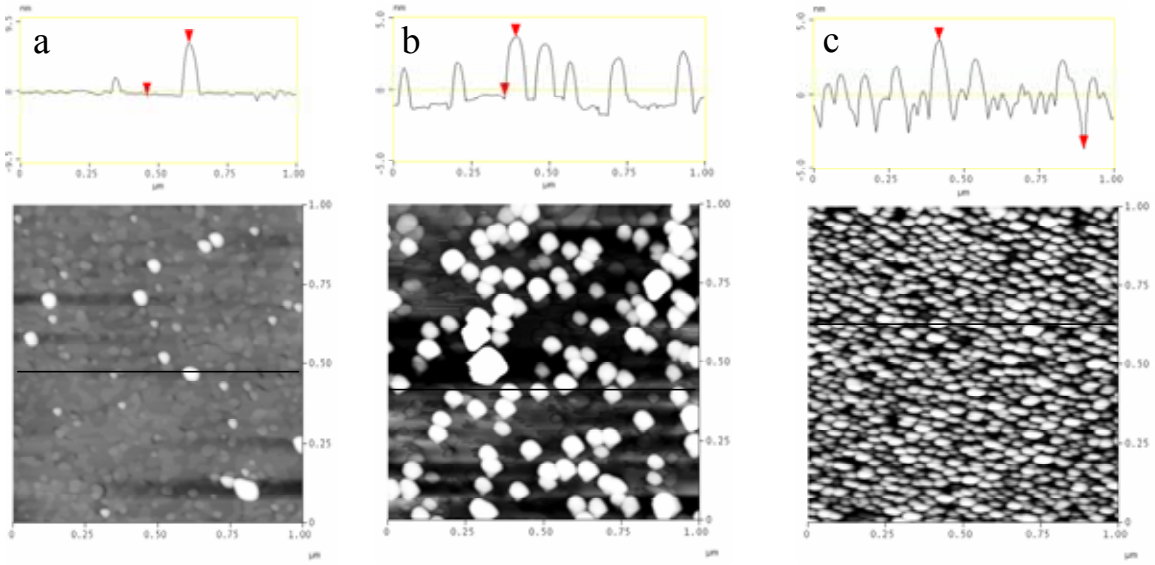

Figure 3. AFM images of InGaAs surface as a function of AsH3 partial pressure at 500°C for a 4.5 nm InGaAs deposition. The AsH3 partial pressure used was a) 0.14 torr, b) 0.06 torr, and c) 0.02 torr. Top sections showing topography correspond to the horizontal line across each image. The vertical image scales are 20 nm for a and 10 nm for b and c.

lowering the AsH_3 partial pressure at a growth temperature of 500°C. Figure 3a corresponds to a factor of two reduction in the AsH_3 partial pressure to 0.14 torr. Islands formed are 40 by 30 nm to 60 by 50 nm in lateral extent with heights comparable to those observed in Figure 2c, 5 ± 2 nm. The density of islands is low, about 30 μm^{-2}. Figure 3b shows the surface obtained

for an AsH_3 partial pressure of 0.06 torr. The island density is 120 μm^{-2} and the lateral extent is 50 by 30 nm to 70 by 50 nm, with island heights of 5 ± 1 nm. The AsH_3 partial pressure was reduced further to 0.02 torr producing the surface in Figure 3c. The density of islands has increased to over 500 μm^{-2} and the lateral dimensions and height are comparable to those shown in Figure 2c given the uncertainties in evaluating these parameters due to the high island density. The trend observed suggests that the threshold for island formation is dependent on the AsH_3 partial pressure and lower AsH_3 partial pressures induce higher island densities.

The driving force for the two-dimensional to three-dimensional transformation is the lower total energy state obtained when islanding occurs relative to the energy of the planar film. Decreasing the thickness of the deposit should recover planar growth. This experiment was performed for at 500°C and 0.02 torr AsH_3 partial pressure. Figure 4 shows the evolution of island density. A high density of islands is retained for InGaAs thickness of 3 nm and above as shown in Figure 4a. At 2 nm of growth, the density of islands decreases, but is still high at

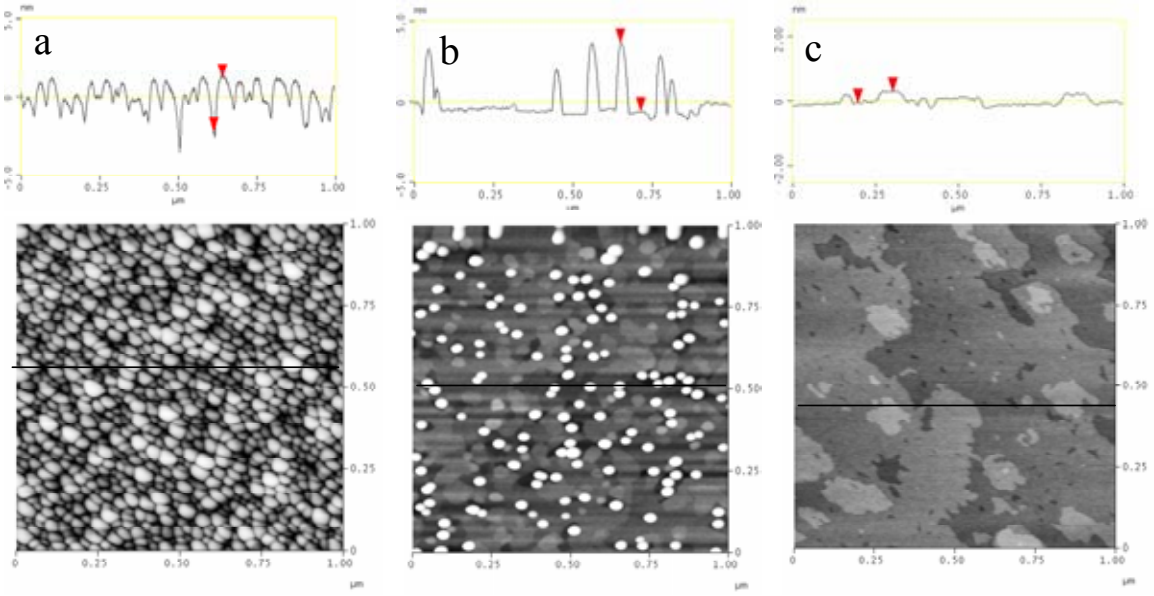

Figure 4. AFM images of InGaAs surface as a function of the thickness of InGaAs at 500°C and 0.02 torr AsH_3. The InGaAs thicknesses are a) 3.0 nm, b) 2.0 nm, c) 1.5 nm. Top sections showing topography correspond to the horizontal line across each image. The vertical image scales are 10 nm for a and b and 5 nm for image.

140 μm^{-2} (Figure 4b). The size of the islands range from 30 by 20 nm to 50 × 35 nm in lateral extent with heights of 3 to 5 nm. Growth of 1.5 nm of $In_{0.4}Ga_{0.6}$. As, shown in Figure 4c, results in large two-dimensional islands with a density of 40 μm^{-2}, lower in density and larger than the two-dimensional islands shown in Figure 2b. In addition to the monolayer thick islands, small monolayer deep pits are formed on the surface with a density of 80 μm^{-2}. The formation of pits on strained films has been shown to be a mechanism for strain relief [20]. Further information about the transition from a planar quantum well (QW) to a SAQD can be determined by PL. Figure 5 shows the evolution of the PL emission at room temperature for the samples shown in Figure 4. The two peaks are observed for the sample with 2.0 nm of InGaAs, one at 1287 meV and another at 1132 meV. The two features are attributed to the coexistence of SAQD with a QW. The energy of 1287 meV is consistent with energy of segregated QW with a 2.0 nm thickness. Increasing the InGaAs thickness to 3.0 nm results in a dramatic decline of the QW emission, which now appears as a high energy shoulder in the spectrum. The QW emission energy has increased, consistent with conversion of the material from the QW to SAQD. The SAQD emission has blue-shifted to 1155 meV. Increasing the thickness to 3.4 nm further quenches the QW emission at 1356 meV, which corresponds to a 0.5 nm QW. A small red-shift (24 meV) is observed going from 3 to 3.4 nm of InGaAs and the peak energy saturates at 1132 meV for thicknesses exceeding 3.4 nm.

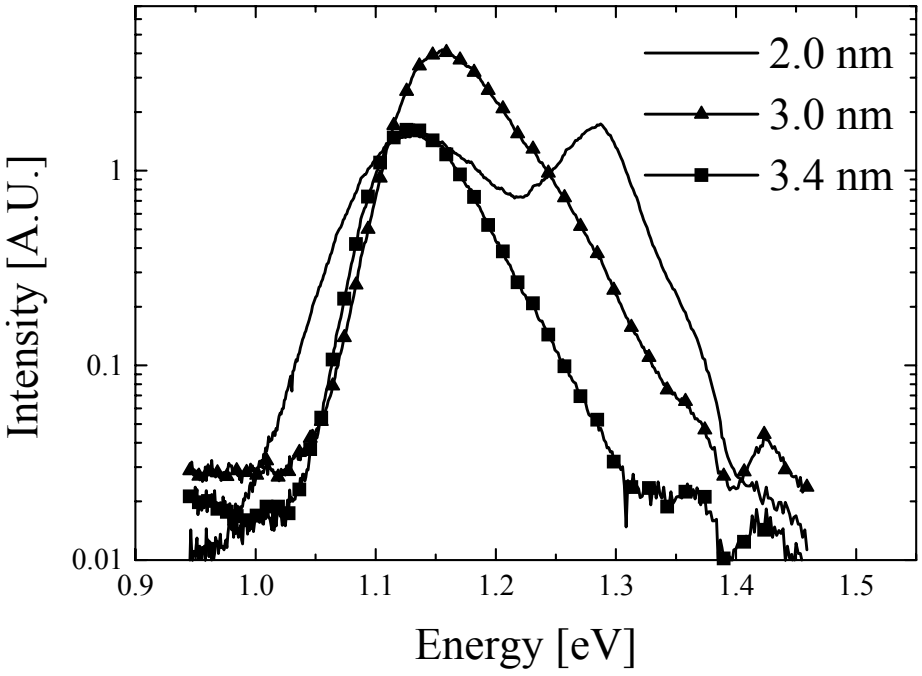

Figure 5. PL spectra of InGaAs grown using 0.02 torr AsH3 at 500°C buried in GaAs. The energy levels in the QD are changed as the segregation thickness is exceeded (3.4 and 3.0 nm). For thickness of 2.0 nm the required segregated thickness has not been achieved so few QD are formed and the emission is dominated by the emission from the wetting layer or QW.

The combined results suggest that high AsH_3 partial pressures and low growth temperatures stabilize planar growth of strained layers that would otherwise undergo three-dimensional transformation under different conditions. These results are not the first to suggest that SAQD formation can be impacted by the magnitude of the AsH_3 partial pressure. Investigations of $In_{0.5}Ga_{0.5}As$ on GaAs (001) have shown that more material is required to nucleate SAQD under high AsH_3 partial pressure conditions than for SAQD grown under low AsH_3 partial pressures for similar conditions. The SAQD formed under higher AsH_3 partial pressures had lower densities than the ones grown under low partial pressure conditions [17]. These results are consistent with my observations. These observations are explained by

postulating that indium can segregate to the surface and promote the transformation of the morphology forming SAQD.

3.1.3 Discussion

The amount of surface enrichment, or segregation, depends on the growth conditions (growth temperature and AsH_3 partial pressure) and the magnitude of the coherency strain of the film to the substrate. The phenomenological model used to describe surface enrichment introduces a segregation coefficient, *R* [8, 12]. Physically *R* is related to the distance δ (in monolayers) over which segregation effects are operative through $R = e^{-1/\delta}$. A large *R* indicates a large segregation effect, while a small *R* indicates little segregation is occurring. The composition of the *n*th deposited monolayer is given by [11]:

$$X_n^w = X_0(1 - R^n) \tag{1}$$

Where X_0 is the bulk composition associated with the growth conditions used. The alloy grown will reach the bulk composition only after the deposition of several monolayers. The dependence of this quantity on deposited thickness is shown in Figure 6. The non-volatile material that is not incorporated into the film is left on the surface. The thickness of this segregation layer, in monolayers, is given by [11]:

$$MFI_n = X_0 \frac{(1 - R^n)}{1 - R} \tag{2}$$

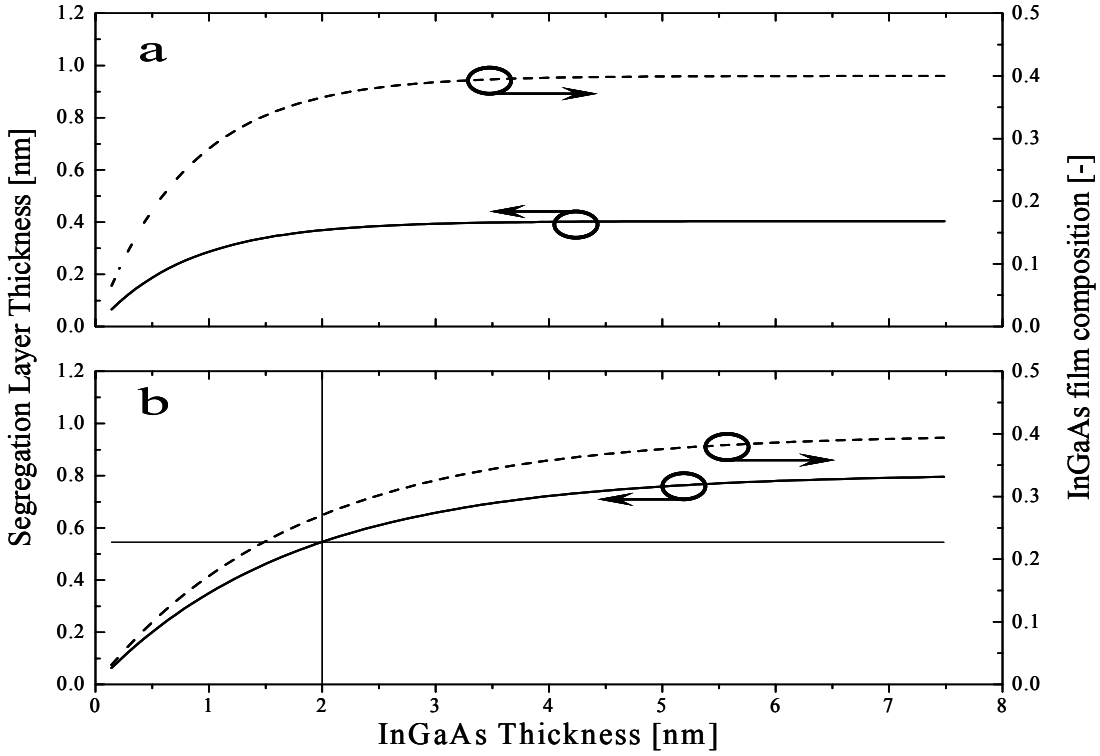

Figure 6. The segregation coefficient, determined by the growth conditions, sets the composition profile obtained and the final thickness of the segregated layer on the surface. Low values of segregation coefficient (R = 0.7 in a) produce an abrupt profile that achieves the desired composition after 3 nm of growth with a small segregated layer thickness (0.4 nm). Larger values (R = 0.85 in b) produce a graded profile with a large segregation layer thickness, resulting in three-dimensional growth when the transition thickness is reached. The density of islands formed depends on the amount of segregation layer available.

The segregation layer thickness is plotted on the opposite ordinate axis in Figure 6. Under certain conditions the thickness of the segregated region is very low (~ 1 ML) as shown in Figure 6a. Conditions that minimize the concentration of group III adatoms on the surface: low growth temperatures and high AsH_3 partial pressures, have low values for the segregation coefficient. Conditions that increase adatom concentrations: high growth temperatures and low AsH_3 partial pressures have higher values of the segregation coefficient.[21] Analytical treatments on the transition thickness from two-dimensional to three-dimensional growth suggest that for the strain associated with $In_{0.4}Ga_{0.6}As$ relative to the GaAs substrate (0.028

compressive), the transition thickness should be 2 to 3 nm.[22,23] These theories are based on the energy of the islanded surface relative to the strained planar surface. Thermodynamic analysis of the two-dimensional to three-dimensional transition proposes that a "liquid" or amorphous layer is present on the surface of highly strained films, enabling the large scale mass transport that occurs when QD are formed [14]. For conditions generating large values of *R*, the segregation layer grows and enables the three-dimensional morphology to be generated. The results shown in Figure 6b predict it takes a 0.6 nm segregation layer for the surface to undergo a transition to a three-dimensional morphology. Slightly different growth conditions result in smaller values of *R*, and produce planar surfaces as observed for Figure 6b. In MOCVD the arsenic incorporation is coupled to the growth temperature, since low temperatures limit AsH_3 thermal decomposition and lower the effective arsenic incorporation to the surface. This is believed to be the case for the surface shown in Figure 2a grown at 450°C with an AsH_3 partial pressure of 0.27 torr. If the arsenic incorporation could be controlled independently of the growth temperature, the value of R achieved at 500°C planar growth would be expected at 450°C resulting in planar growth.

The apparent discrepancy of the results presented here with the literature on this topic should be addressed. Previous studies have identified that group III stabilized surfaces are stable against island formation while arsenic stabilized surfaces are not [24]. These results do not contradict previous observations, but suggest that extremely arsenic enriched heterostructure surfaces found in the MOVPE environment can be stable against islanding, in contrast to the less arsenic rich MBE surfaces that almost categorically form QD for $In_{0.4}Ga_{0.6}As$ deposition on GaAs.

Subsequent layers deposited on the enriched segregation layer will incorporate the material forming an interface with a graded composition given by:

$$X_n^b = X_0(1-R^N)R^{n-N} \tag{3}$$

Where N is the number of monolayers of the alloy deposited before the composition is changed. The well and barrier composition profiles can be modeled using equations (1) and (3) and used to compute a one-dimensional potential for the segregated QW. The ground state energies for segregated QW have been calculated as a function of the deposited alloy thickness using variational techniques with a Gaussian trial function [25]. The results of this calculation as a function of InGaAs thickness for R = 0.7, corresponding to a δ = 2.8 monolayers or 0.8 nm, are shown in Figure 7. Also shown are the results for an abrupt QW model. The emission energy for the segregated well is higher than the abrupt model for small thicknesses, but converges to the bulk bandgap for large values of the InGaAs thickness. Figure 7 also summarizes the experimental emission energy for samples grown at 500°C with low and high AsH_3 partial pressures. The full widths at half maximum (FWHM) for the peaks observed are plotted on the right ordinate axis of Figure 7. The FWHM for the high AsH_3 partial pressure samples are nearly constant at 38 meV. These results are in contrast to the samples grown under low AsH_3 partial pressure at the same temperature. The linewidths for these samples are broad, consistent with an inhomogeneous distribution of ground state energies. The dependence on thickness is different for the two conditions. The energy of the low AsH_3 partial pressure is nearly independent of InGaAs thickness with the FWHM decreasing for thicker structures. This trend is consistent with restricted expansion of the SAQD size with increases in the amount of material deposited. The emission energies for the high AsH_3 partial pressure samples decrease nearly monotonically, consistent with the layer thickness determining the transition energy. While the agreement

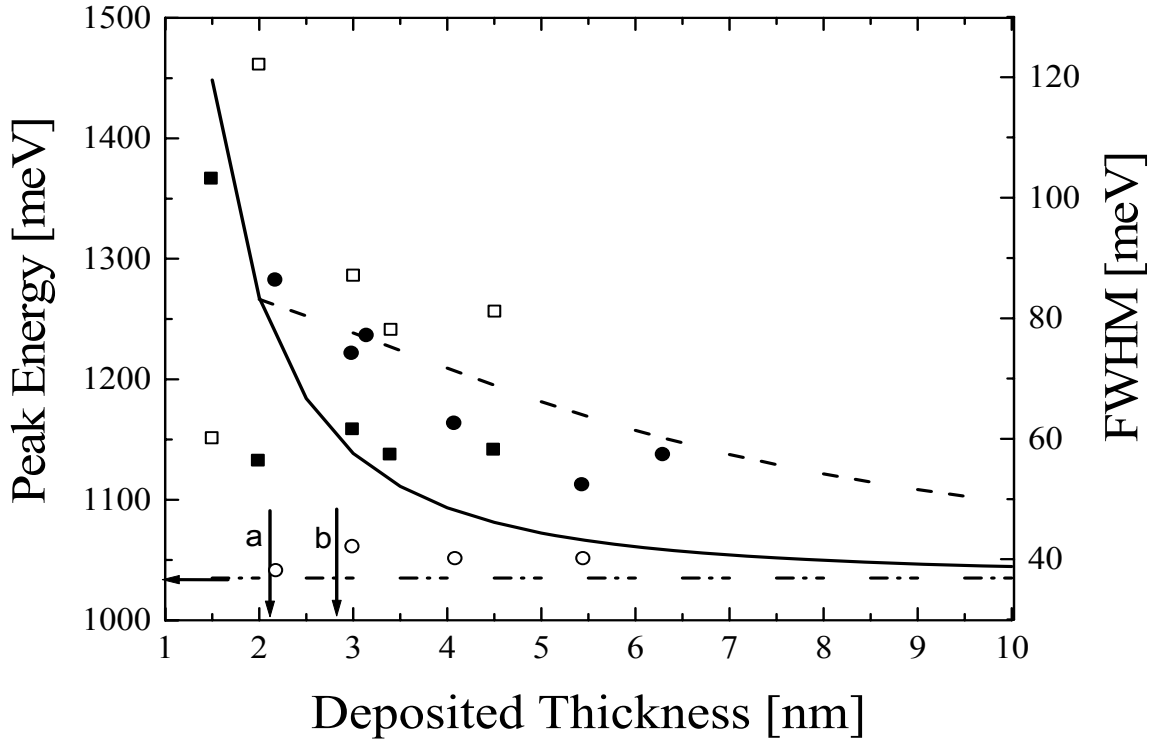

Figure 7. Emission energy of the InGaAs structures grown under high and low AsH_3 partial pressure has different dependences as a function of InGaAs thickness. The following key holds for this figure: high AsH_3 partial pressure results (o - emission energy, □ – FWHM), low AsH_3 partial pressure results (● - emission energy, ■ – FWHM). The solid curve corresponds to the abrupt quantum well ground state energy and the dashed curve corresponds to the segregated solution with R = 0.7. The horizontal dashed-dotted line is the strained bandgap of $In_{0.40}Ga_{0.60}As$ on GaAs. The vertical arrows labeled a and b are thermodynamically predicted transition thicknesses.

between the data and the segregated well solution is not exact, it is significantly better than the trend given by the abrupt QW model. These observations support the conclusion that segregation is active in the growth of InGaAs on GaAs by MOCVD.

The thickness of the segregation layer is correlated to density of islands. Larger segregation layers appear to produce denser ensembles of islands that are more uniform lateral extent and height. This is difficult to access quantitatively due to the high density of the islands in Figures 2 and 3. The segregation layer in all cases is less than the amount of material present

in the ensemble of QD. This is consistent with the observations made by TEM that material from the GaAs buffer layer or the InGaAs epilayer is incorporated into the QD during formation.

3.1.4 Conclusions

The formation of $In_{0.4}Ga_{0.6}As$ QD by MOVPE has been studied. The conditions for QD formation have been mapped out experimentally. High growth temperatures (550°C and above) and low AsH_3 partial pressures (below 0.14 torr) promote the three-dimensional transformation. Lower temperatures (500°C and below) and high AsH_3 partial pressures (0.28 torr and above) inhibit the three-dimensional transformation. These observations were interpreted in terms of the formation of a surface segregation layer that builds up on the surface of the growing crystal. For the InGaAs composition investigated the critical segregation thickness predicted to be 0.6 nm. The material incorporated into the islands is in excess of the material present in the segregation layer, suggesting that portions of the crystalline layer formed during epitaxy and the underlying layers of GaAs are incorporated into the islands formed.

3.2 Growth investigations on InAs binary SAQD

Quantum dots (QDs) and other nanostructures provide an additional degree of freedom in the design of semiconductor devices and heterostructures. Quantum confinement in three dimensions produces changes to the energy levels and carrier density of states. QD can be formed through the two-dimensional to three-dimensional growth transformation that occurs for highly strained films, known as Stranski-Kranstanov growth mode. The islands formed are believed to coexist with a thin, low indium-content wetting layer that has less strain than the original strained film.[26,27] The formation of quantum dots is extremely sensitive to a wide variety of parameters in both MBE or MOCVD.[28,29] From the initial buffer layer morphology through all the parameters that go into their growth and formation, to the procedure used to cap

the structures, all parameters and steps have a large impact on the energy levels of the quantum dots. We have conducted studies on the growth of InAs QD on GaAs using metal-organic chemical vapor deposition (MOCVD). This report will concentrate on the effect that the growth parameters of deposited InAs thickness, temperature, growth rate, and AsH_3 partial pressure, have on the ground states and morphology of InAs QD. During our studies we have found conditions that produce 1.3 μm emission. For conditions which produce 1.3 μm emission, we have investigated the effect different capping layers of InGaAs and GaAsSb have on the QD energy levels relative to GaAs.

3.2.1 Experimental Details

Metal-organic chemical vapor deposition (MOCVD) was used for the deposition of the QD structures. Table I contains the details associated with the structure grown for our investigations with the nominal growth rates and hydride partial pressures used. A thick GaAs buffer was grown at 650°C on near singular GaAs(100) ± 0.1° and then cooled to 600°C for growth of a 300 nm $Al_{0.60}Ga_{0.40}As$ cladding and a 70 nm GaAs nucleation layer. We have found that InAs QDs nucleate more uniformly on GaAs layers that exhibit step flow growth with wide terraces than on surfaces that are grown at lower temperature that exhibit two dimensional island growth. The structure grown at 600°C was cooled to the temperature desired for QD growth. We varied this temperature between 480 and 520°C to evaluate the effect of temperature on QD formation. After the InAs deposition the metal-organics and AsH_3 were removed from the reactor and the film was annealed for 10 seconds in hydrogen. AsH_3 was then reintroduced into the reactor for 2 seconds and followed by the growth of a 5 nm GaAs layer at the temperature of InAs growth to encapsulate the QDs. The temperature of the sample was ramped to 600°C for growth of the remainder of the GaAs cap (65 nm) and a symmetric $Al_{0.60}Ga_{0.40}As$ cladding.

The nominal growth rate of InAs was varied from 0.25 to 1.9 Å/second and the thickness of InAs deposited was varied from 5.5 Å to 7.5 Å to determine if increasing the amount of InAs can generate larger QDs. Quantum mechanical arguments suggest that larger QDs have smaller ground state energies than the smaller QDs and should shift emission to longer wavelengths. This red shift has been observed experimentally of InAs QD.[30] The partial pressure of AsH_3 was varied from 8×10^{-3} torr to 0.42 torr during the growth and annealing of InAs. The low temperature (LT) GaAs cap grown after InAs deposition and QD formation was grown with an AsH_3 partial pressure of at least 0.21 torr to insure that non-stoichiometric defects are not introduced during growth.

Results from the literature suggest that the composition and strain state of the layer used to cap the QDs can change the ground state energies. InGaAs alloys with low indium composition have been investigated extensively to reduce the strain imposed on the QD by the surrounding material and minimize interdiffusion of indium in the QD. [31,32] We have compared the standard GaAs cap to $In_{0.1}Ga_{0.9}$ As and $GaAs_{0.9}Sb_{0.1}$. Use of the later material has not been reported previously for capping InAs QDs. For these experiments the thickness of the cap has been held constant at 5 nm.

TMIn, TEGa, and EDMAAl were used for the group III precursors and 100 percent AsH_3 was the group V precursor. The reactor was a high speed rotating disk system operated at 900 rpm and 70 torr. The growth rates and nominal thicknesses used for layers beside the InAs QD layer were held constant and are shown in Table I along with the partial pressure of hydrides used. For some samples, uncapped QDs were grown on top of the high temperature (HT) GaAs cap layer to allow the size of the QDs to be estimated. The procedure for forming the uncovered surface QDs was the same as for the QD covered with the LT GaAs cap, except instead of

covering sample with an additional layer the sample was cooled down to 300°C under an AsH_3 overpressure. Room temperature photoluminescence (RT PL) was excited by a 780 nm laser diode to observe of the energy levels in the QDs. Atomic force microscopy (AFM) performed in tapping mode using Si tips was performed to image the surface QDs that were grown on top the structure described in Table I.

Table I. Nominal growth conditions for the structure investigated. The thicker high temperature (HT) GaAs cap layer was grown when InAs QDs were nucleated on top of the structure for investigation by AFM.

Layer Description	Thickness [nm]	Growth Rate [Å/second]	Growth Temperature [°C]	AsH_3 Partial Pressure [torr]
HT GaAs cap	20 – 70	2	600	0.42
$Al_{0.60}Ga_{0.40}As$ cladding	300	5	600	0.42
GaAs spacer	65	2	600	0.42
LT GaAs cap	5	2	varied	At least 0.21
InAs QD layer	varied	varied	varied	varied
GaAs nucleation layer	70	2	600	0.42
$Al_{0.60}Ga_{0.40}As$ cladding	300	5	600	0.42
GaAs buffer layer	200	7	650	0.42

3.2.2 Results and Discussion

Our initial effort was to look at the effect of the thickness of InAs deposited on the QD energy levels. Spectrum 1 shown in Figure 8 was observed at 1270 nm (980 meV) for an InAs thickness of 6 Å grown at 500°C. The amount of InAs was increased to 6.6 Å to determine if emission at longer wavelengths could be obtained at a QD growth temperature of 500°C. Spectrum 2 is the result, is also shown in Figure 8, and shows that the QD-related PL has been quenched. This result suggests that the QD formed with a 6 Å deposition are near their maximum size and the additional 0.6 Å of InAs results in a loss of coherency of the QD. The incoherent QDs contain dislocations that act as non-radiative recombination centers that compete

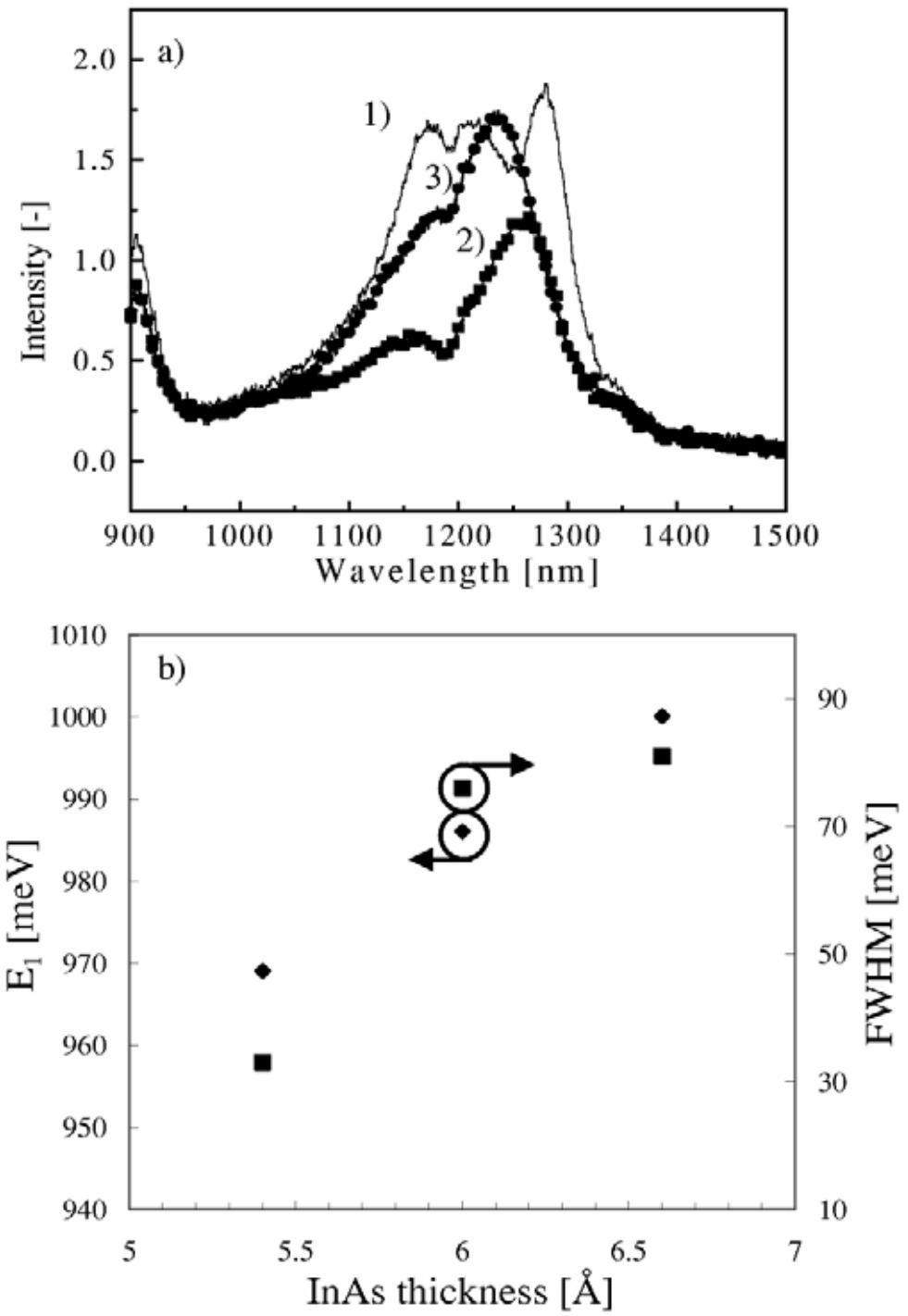

Figure 9. a)RT PL spectra for InAs QD grown at 480°C using 1) 5.4 Å of InAs(——), 2) 6.0 Å of InAs(—■—), and 3) 6.6 Å of InAs (—●—). b) The shifts in the ground state energy with increasing InAs correspond in an increase in the FWHM of the ground state transition. The blue shift observed suggests that other factors impact the ground state energies.

with the radiative pathway through the smaller QD. The transformation of coherent, optically active QDs to incoherent, dislocated QDs can be suppressed by lowering the QD growth temperature. This is due to the reduced indium adatom surface diffusion at lower growth temperatures.[33,34] Using a temperature of 480°C instead of 500°C allows the QD to remain coherent and optically active for thicker InAs deposits as shown by the spectra in Figure 9a. However, the energy levels are not modified in the manner initially proposed. For 5.4 Å of InAs (Figure 9a, Spectrum 1) we observe well resolved ground, first, and second excited states at 1280 nm (980 meV), 1230 nm (1010 meV), and 1170 nm (1060 meV), respectively. As shown in Figure 9a, Spectrum 2, the addition of 0.6 Å of InAs results in a single peak with a well defined shoulder that is blue shifted relative to the ground state observed for the 5.4 Å sample to 1260 nm (990 meV). This effect persists at 6.6 Å of InAs, with a blue shift of the RT PL to 1240 nm (1000 meV) as shown by Figure 9a, Spectrum 3. Figure 9b summarizes the spectra presented in Figure 9a and shows that as the ground state energy shifts to higher energies with increasing deposit thickness the FWHM increases. These observations suggest that the size of coherent QDs and the ground state energy is not monotonic with the amount of InAs deposited and additional input is needed to understand how the QD are changing as the amount of InAs deposited increases. Figure 10 shows two AFM images of the QD formed with 5.4 Å and 6.6 Å of InAs at 480°C. At 5.4 Å of InAs a single distribution of island heights with average height of 3 nm, base diameters of 40 nm, and a density of 30 μm^{-2} is formed. A small density (1 μm^{-2}) of large islands is formed that are 23 nm high and 75 nm at the base. By comparison the sample with 6.6 Å of InAs has a bimodal distribution of island heights.

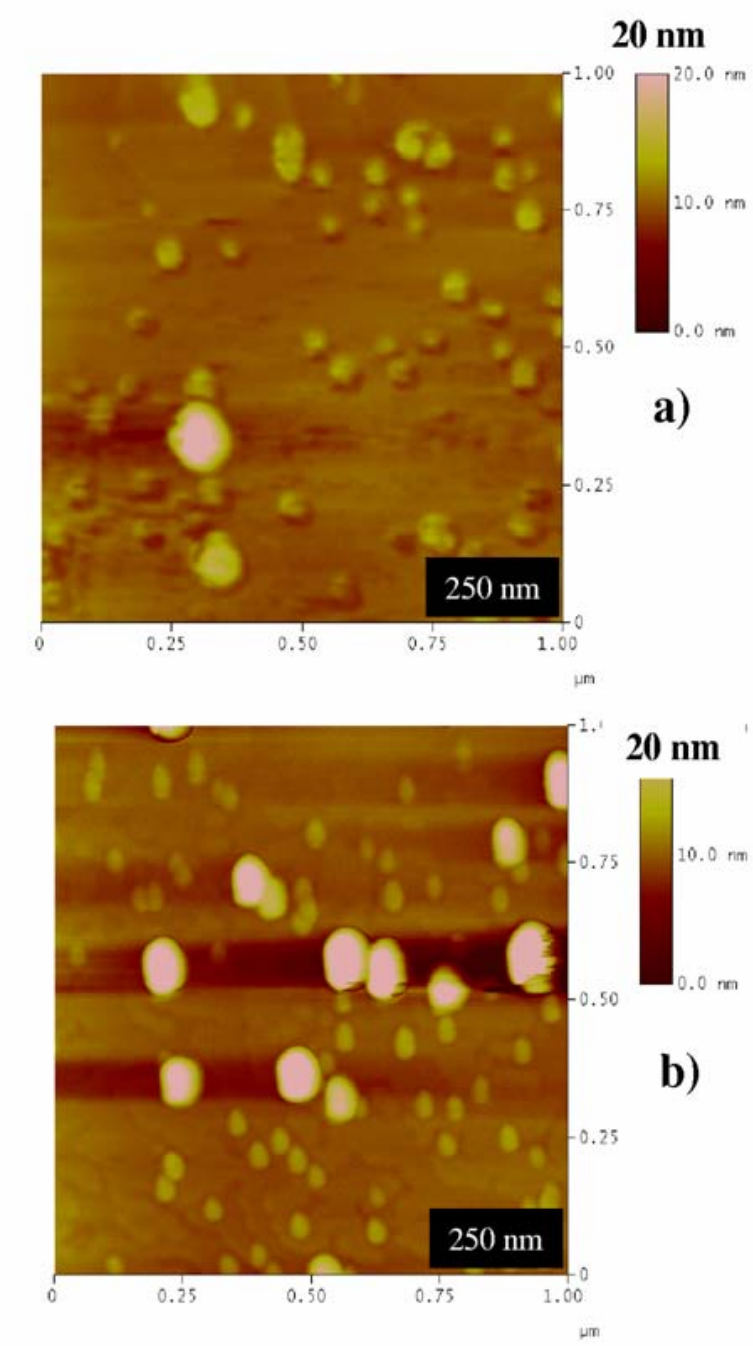

Figure 10. AFM micrographs of uncapped QD formed with a) 5.4 Å of InAs and b) 6.6 Å of InAs. For a) the islands are 3.0 nm high with a base of 40 nm and a density of 30 µm-2. For b) the two sizes of islands exist: small islands 3.3 nm high with as based diameter of 30 nm and a density of 30 µm-2 and larger islands 12 nm higher with 75 nm base diameter and a density of 10 µm-2. This result suggests that the island height is not the only geometric parameter that impacts the QD energy levels.

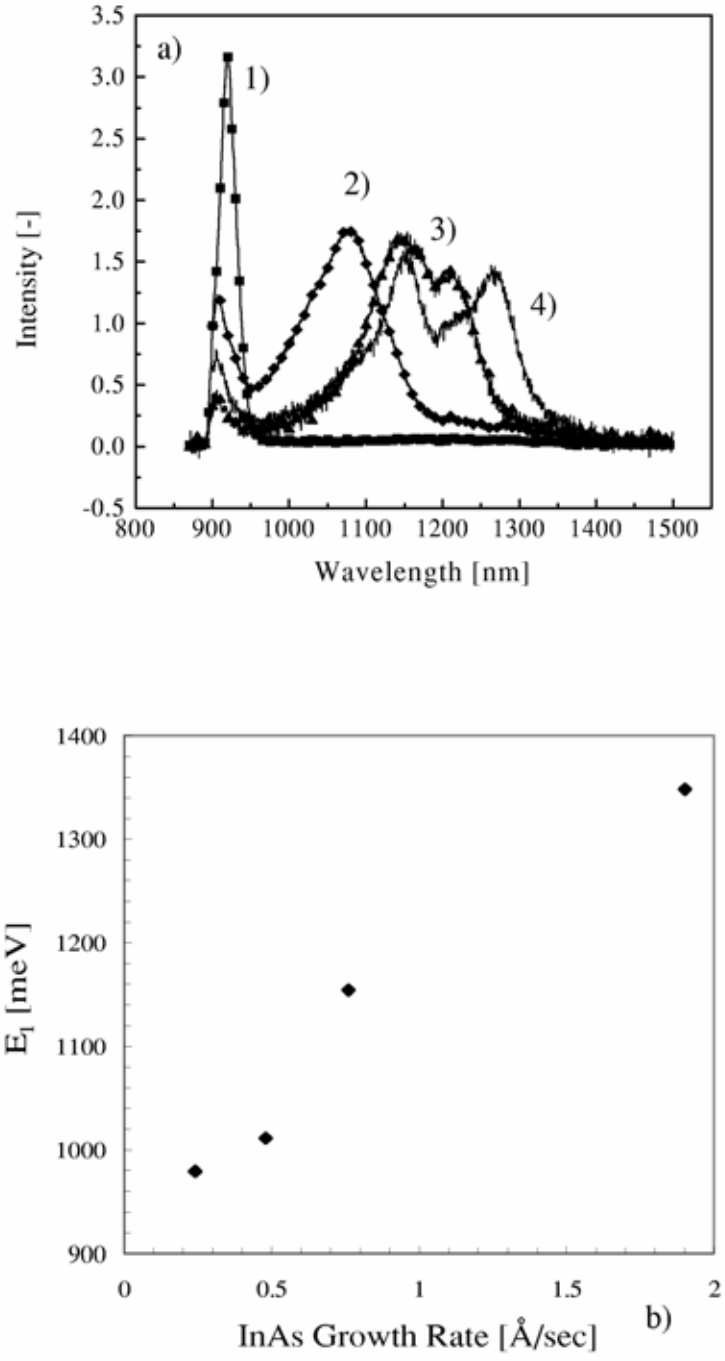

Figure 11. a) RT PL spectra of InAs QD grown at 500°C with a InAs thickness of 6 Å using different InAs growth rates: 1) 1.9 Å/second(___■____), 2) 0.75 Å/second (___♦____), 3) 0.48 Å/second (___▲____), and 4) 0.24 Å/second (_____). The red shift, interpreted as larger island size, observed with decreasing growth rate, follows from kinetic theories of QD nucleation. Spectra 3) and 4) are multiplied by a factor of five to compare them with spectra 1) and 2), suggesting that the areal density of islands is less for samples grown at lower growth rates. b) An over 400 meV shift in the ground state transition is observed for the range of growth rates investigated.

The small islands are 3.3 nm high, a base of 30 nm, and a density of 30 μm^{-2}. The larger islands are 12 nm high, with a 75 nm based, and a density of 10 μm^{-2}. The small islands are likely coherent and contribute to the optical response, while the large islands have grown so large that they are probably not coherent. While the 6.6 Å sample has small QDs that are taller, the average base diameter has decreased, presumably due to mass transport to the large islands. The small islands formed for the 5.4 Å deposition are closer to circular in lateral extent, while the small islands formed for the 6.6 Å deposit are elongated along the [0-11] direction. This suggests that the height of the QD is not the only parameter that controls the energy levels in the QD and that the aspect ratio, defined as the height divided by the base diameter, and the island symmetry can impact the energy levels.

Investigations of the impact of InAs growth rate were performed at a temperature of 500°C using an InAs thickness of 6 Å. Figure 11a shows the modifications to the spectra as the growth rate is decreased from 1.9 Å/second (Spectrum 1) to 0.24 Å/second (Spectrum 4). The decrease in the ground state emission wavelength with increasing growth rate is attributed to a decrease in the QD size and can be accounted for with kinetic nucleation theory.[33,35,36] This theory predicts an increase in the density of the QDs along with a reduction in lateral dimension with increased growth rate. The larger QDs are formed at low growth rates and have smaller ground state energies than the smaller QD formed at higher InAs growth rates as shown in Figure 11b.[37] The trend of higher QD density at higher growth rate is observed in the factor of five increase in the RT PL intensity observed for the two samples grown at the highest growth rates (Spectra 1 and 2).[38,39]

The effect of AsH_3 partial pressure on the QD growth was evaluated at 500°C for 6 Å of InAs. MBE investigations suggest that As_4 flux has a nonlinear effect on the QD PL wavelength,

producing a decrease in wavelength as the As_4 flux is increased for low fluxes and producing a increase in wavelength for the highest As_4 fluxes investigated.[40] Our investigations have produced a similar dependence as shown in Figure 12. We observe a dramatic decrease in the ground state energy as the AsH_3 partial pressure is increased from 8×10^{-3} torr to 0.05 torr. The ground state energy appears to stabilize as the AsH_3 partial pressure is increased further. The mechanism for this effect is unclear. By increasing the AsH_3 partial pressure the incorporation

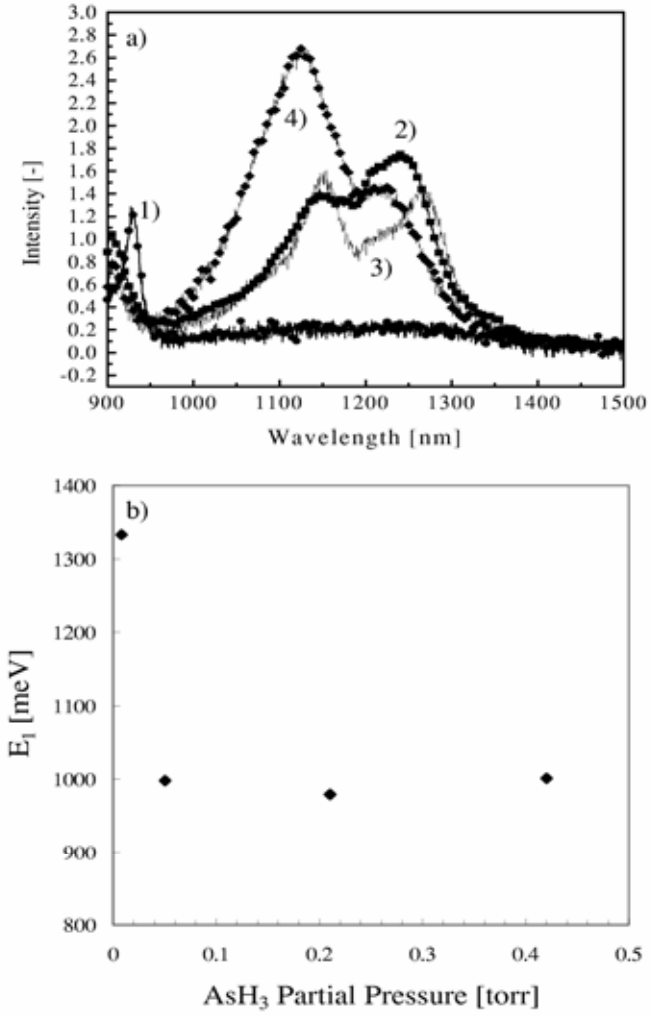

Figure 12. a) RT PL spectra of InAs QD grown at 500°C with a InAs thickness of 6 Å using different AsH_3 partial pressures: 1) 8×10^{-3} torr (—●——), 2) 0.05 torr(—■——), 3) 0.21 torr (——), and 4) 0.42 torr(— ◆——). b) The trend for the ground state energy is plotted as a function of the AsH_4 partial pressure. The nonlinear shift of the ground state energy is similar to what has been observed for MBE.

length, the distance an indium adatom travels before incorporating is decreasing.[41] The result of smaller incorporation lengths should be smaller, denser QDs resulting in a spectral blue shift. The red shift observed suggests that we are enhancing adatom diffusion on the surface at higher AsH_3 partial pressures compared to the low partial pressure case allowing large QDs to form. The strain state of the QD and its intermixing with surrounding layers impacts the energy levels observed. By adding a small amount of indium to the QD LT cap layer (see Table I) the strain imposed on the QD by the cap can be reduced and the interdiffusion of indium atoms in the QD with the gallium atoms in the cap layer can be reduced. Both of these effects should produce a red shift of the InGaAs capped QD relative to the GaAs capped ones. This is observed experimentally in Figure 13 (Spectrum 2) where the InAs QD capped with $In_{0.1}Ga_{0.9}As$ have a small red-shift relative to the GaAs cap sample. The impact of other capping layers, specifically GaAsSb, has not been investigated. This material can have the same strain as InGaAs, but having two species that can diffuse, antimony and indium, now enhances the interdiffusion. Figure 6 (Spectrum 3) shows RT PL for InAs QDs capped with $GaAs_{0.9}Sb_{0.1}$. The RT PL has broadened significantly, the intensity has been reduced, and the ground state energy is no longer clearly defined. This suggests that the dominant effect of the GaAsSb cap is enhanced interdiffusion with the QD, which results a larger size distribution of QDs and a reduction in the density of optically active QDs. This opposite effect for two cap materials with similar magnitudes of strain suggests that strain reduction of the QD by the alloy cap is not the dominant effect on the QDs and that reduced interdiffusion, in the case of InGaAs, and enhanced interdiffusion for GaAsSb is a large effect.

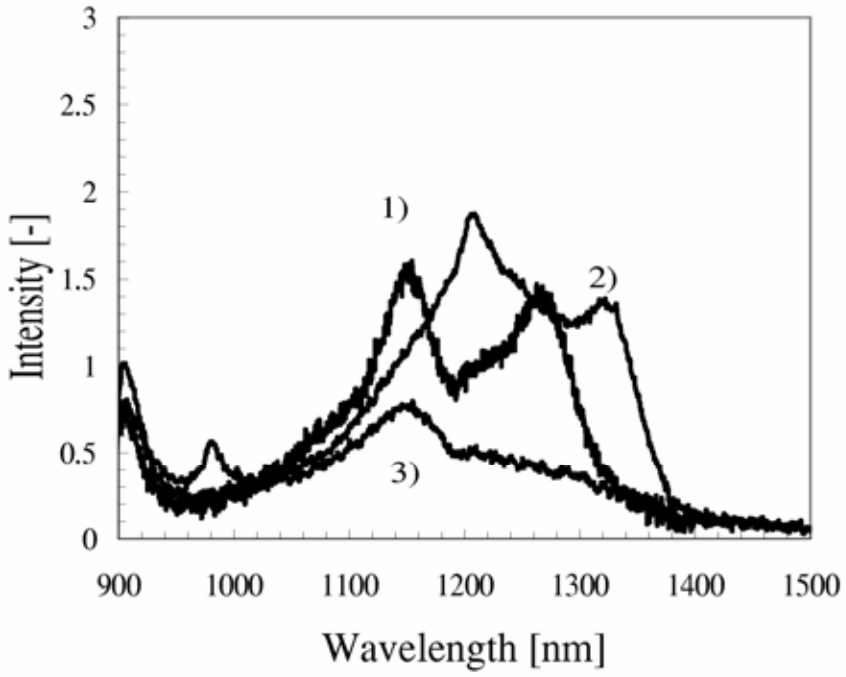

Figure 13. RT PL for different QD cap layers: 1) 5 nm GaAs, 2) 5 nm $In_{0.1}Ga_{0.9}As$, and 3) 5 nm $GaAs_{0.9}Sb_{0.1}$. This suggests that the red shift observed for the $In_{0.1}Ga_{0.9}As$ is due primarly to a reduction in indium interdiffusion and not a strain reduction while the blue shift observed for the $GaAs_{0.9}Sb_{0.1}$ capped sample is due to enhanced interdiffusion and strain reduction has small impact.

3.2.3 Conclusions

InAs QD structures have been grown by MOCVD. The ground state energies of these structures are impacted by many of the growth parameters investigated. In many cases the effects can be explained using the present understanding of island nucleation by the Stranski-Krastanov growth mechanism. The growth of QDs is very sensitive to the growth temperature. No RT PL was observed from samples grown at 520°C, but the window for optically active QD formation increases as the growth temperature is reduced. We were unable to observe a decrease in the QD ground state energy by depositing additional InAs during QD formation, instead a monotonic blue shift was observed with increased InAs thickness at a growth temperature of 480°C. This is attributed to a migration of material from small, coherent QDs to large,

incoherent QDs, resulting in a size decrease for the optically active QDs. We observed a monotonic increase in the ground state energy as the growth rate of InAs used to form the QD was increased. This is related to the decreasing size of the QD at higher growth rates. The AsH_3 partial pressure produces a nonlinear change in the QD ground state energy, producing a dramatic red-shift at low AsH_3 partial pressures and saturating at the highest partial pressures investigated. For capping the QD we have compared the two alloy films, InGaAs and GaAsSb to GaAs. InGaAs capped QD have a lower ground state energy, but a GaAsSb cap produces a broadening of similar transitions observed for GaAs capped QDs. This is attributed to reduction or enhancement in interdiffusion of the QD under different capping conditions.

4.0 OPTICAL INVESTIGATIONS OF SELF-ASSEMBLED QUANTUM DOTS

The theoretical development suggests that QC effects could be observed for realistic homogeneous lifetimes of 100 femtoseconds and inhomogeneous lifetimes of 660 femtoseconds (20 meV). Calculations suggest that Coulomb interactions between populated quantum dots and between the quantum dots and the wetting layer modify the magnitude of the effect and the time scale for observation from what is expected for atomic and molecular systems. These calculations supported our efforts to look for suitable systems to experimental observe QC effects.

Several geometries were investigated for optical investigations are depicted in Figure 14. Normal incidence transmission (Figure 14a) has been used successfully for multiple layer of SAQD (10 or more layers). This convolves the intrinsic effect of the SAQD with the effect of assembling many layers. While this was investigated with a single layer, the measured absorbance was not above the noise level. Slab waveguides with angular end facets (Figure 14b) were investigated to enhance the absorption by increasing the number of passes through a single quantum dot layer. This should have the desired effect, but any resonances in the signal were still overwhelmed by the background absorbance. Planar waveguides (Figure 14c), prepared by polishing crystal edges, proved to be the best geometry for getting large transmission signal from single SAQD layers. Linear absorbance and photoluminescence were used to evaluate the energy states of the quantum dots.

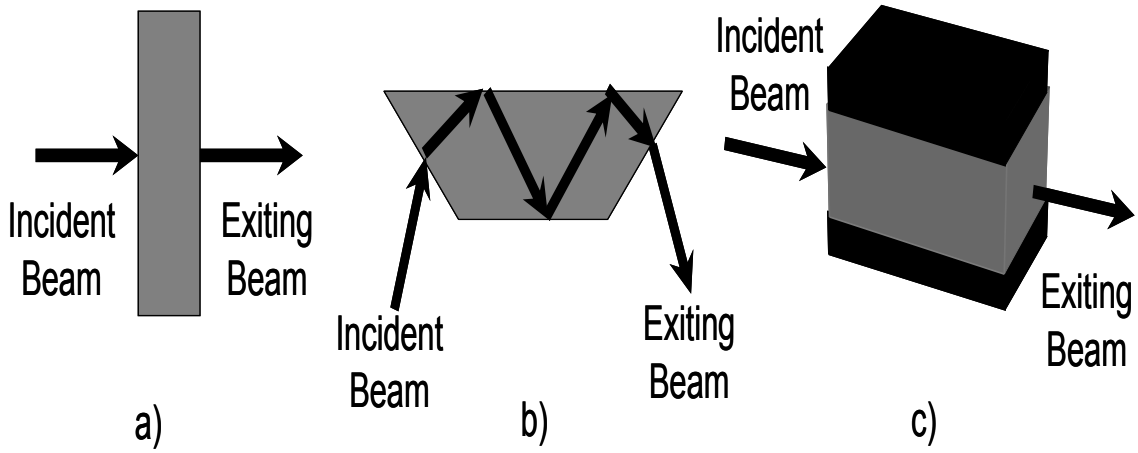

Figure 14. Geometries for optical investigations of SAQD.

To characterize the quantum dot system in the waveguide geometry, we have performed measurements of gain spectra using the established variable stripe length (VSL) technique with optical pumping. We have also developed an extension to the VSL technique which allows us to measure quantitative absorption spectra near the ground state. Typically, it is very difficult to measure linear absorption spectra for quantum dots due to the short interaction length of only a few nanometers when propagating normal to the dot layers. With waveguide absorption measurements, the interaction length is increased, but it is usually not possible to obtain quantitative values of absorption due to uncertainties in waveguide coupling losses. With our technique, we measure the reabsorption of the spontaneous emission generated within the waveguide as an excitation spot is moved relative to the end of the waveguide. Quantitative values of absorption are obtained by fitting the variation in detected intensity versus excitation spot position. Aside from providing sample characterization, these quantitative measurements will be useful both for laser development, and for accurate comparisons with the theoretical models.

Initially, we continued to concentrate on InGaAs quantum dot systems with ground state transitions at 1.34 eV. Figure 15 shows results from the new technique to measure absorption spectra for both TE and TM polarizations in this system (gain spectra were also measured, but are not shown). The narrow linewidth of the ground state transition is promising for QC experiments; however, the lack of excited state resonances makes the identification of a QC level scheme difficult. On the other hand, this system is particularly interesting due to the lack of a clear distinction between isolated quantum dots and a quantum well with additional carrier confinement from interface fluctuations. The experiments so far indicate that this system appears to have properties of both quantum dots and quantum wells. We are further exploring the possibility of using this system in QC experiments using a scheme involving optical transitions with both dot (confined) and well (unconfined) states. We have also performed gain

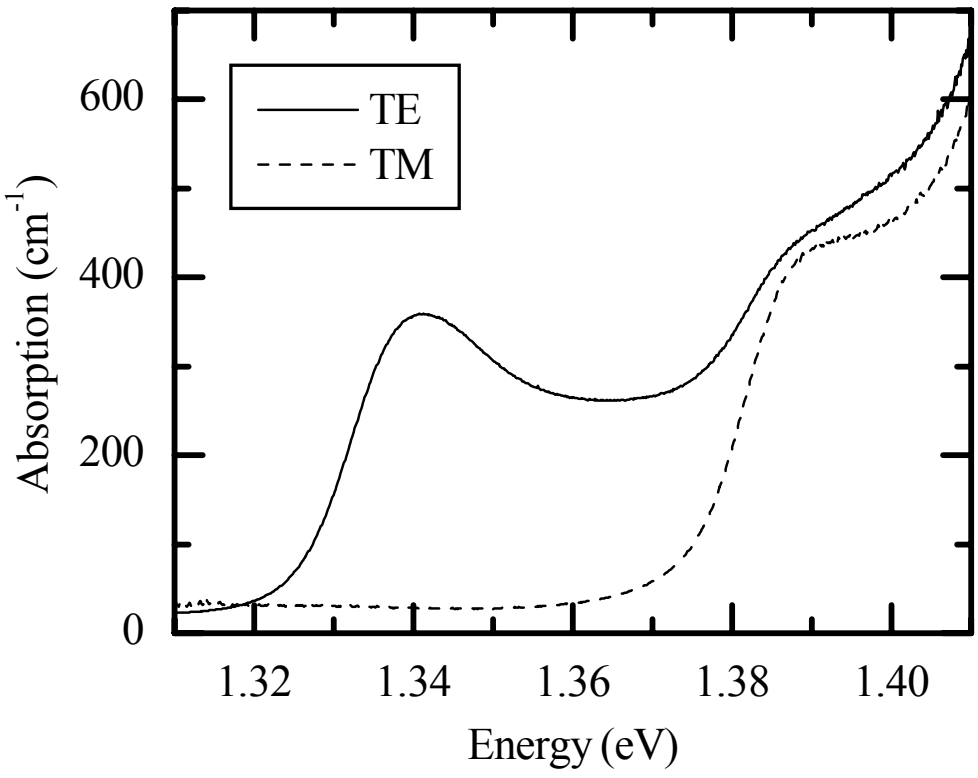

Figure 15. Quantitative TE and TM absorption spectra for weakly confined InGaAs quantum dots.

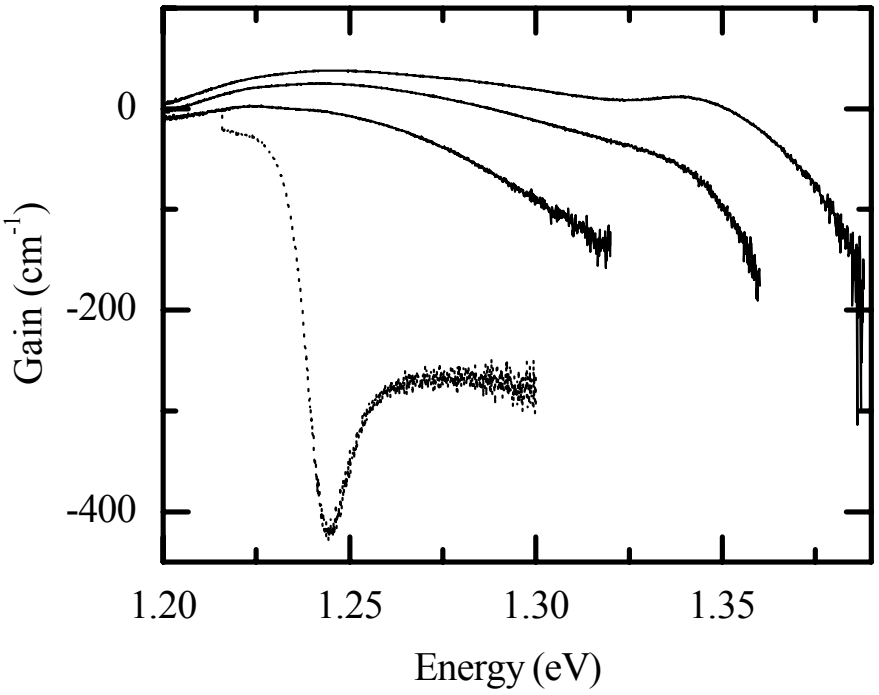

Figure 16. Quantitative TE absorption and gain spectra for InGaAs quantum well. The dotted line shows the linear absorption, and the solid lines show the gain.

and absorption spectra measurements for an InGaAs quantum well system with a ground state transition at 1.25 eV. The results from these measurements are summarized in Figure 16. This system shows a narrow ground state absorption linewidth, and at resonance can be identified. By characterizing this system, we hope to learn about the differences between QC effects in quantum dots versus quantum wells.

We have also performed gain and absorption spectra measurements for an InGaAs quantum well system with a ground state transition at 1.25 eV. The results from these measurements are summarized in Figure 17. This system shows a narrow ground state absorption linewidth, and at resonance can be identified. By characterizing this system, we hope to learn about the differences between QC effects in quantum dots versus quantum wells.

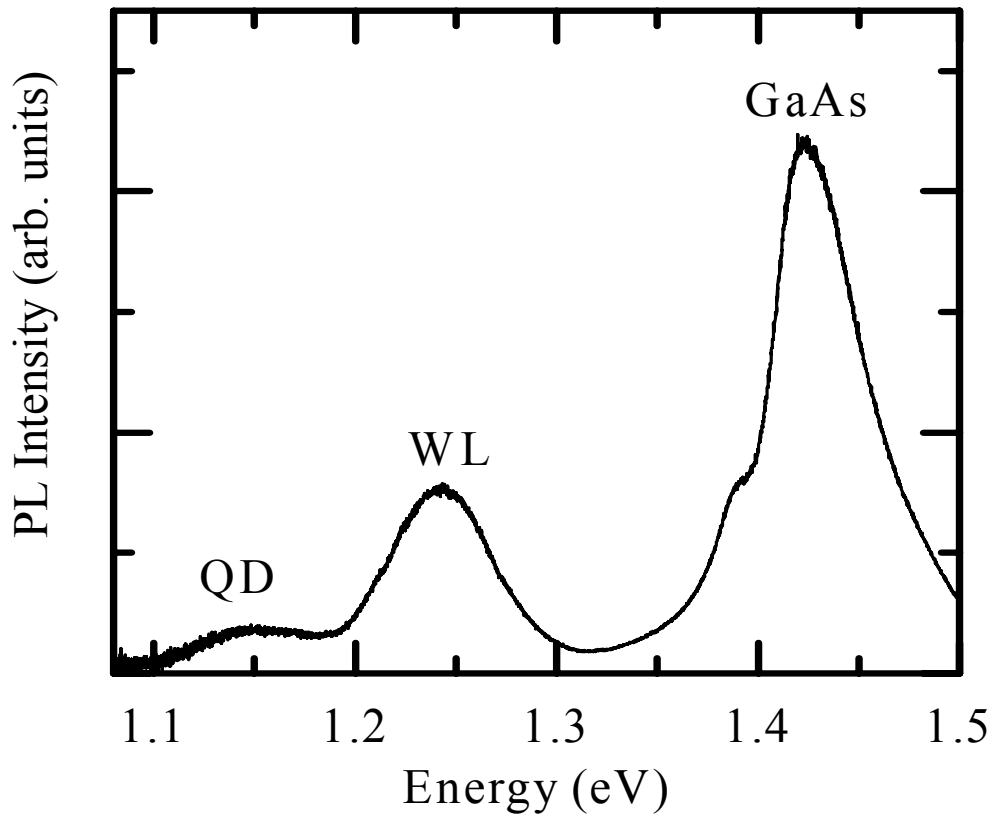

Figure 17. Photoluminescence from InGaAs quantum dots under high pumping intensity. Emission from quantum dots (QD), wetting layer (WL), and bulk GaAs is labeled.

The final InGaAs system studied consists of distinct quantum dots with a ground state transition at 1.15 eV. Attempts to measure absorption and gain spectra failed due to a decrease in detector response at these energies. However, measurements of PL spectra under high excitation levels were obtained, and are shown in Figure 18. The spectrum shows a well-resolved quantum dot transition at 1.15 eV, and a wetting-layer transition at 1.25 eV (identified through comparison with the InGaAs quantum well discussed above), but no quantum dot excited state transitions.

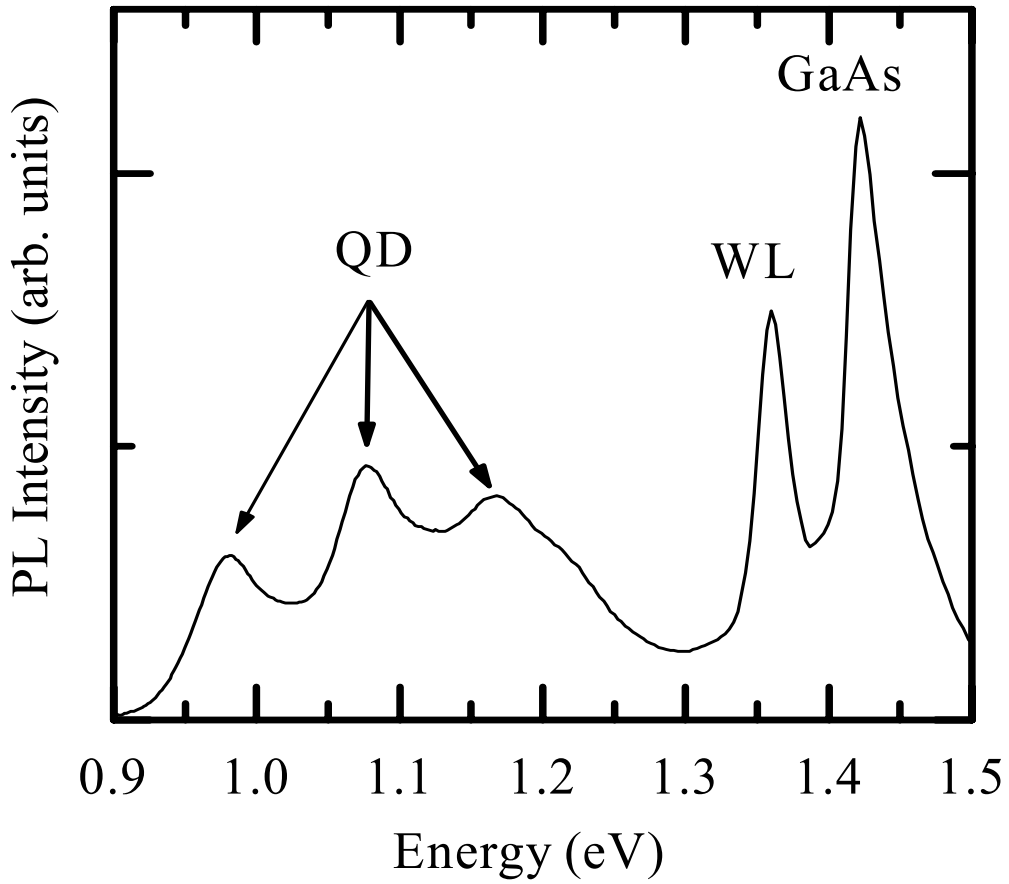

Figure 18. Photoluminescence spectrum from InAs quantum dots under high pumping intensity. Emission from quantum dot states (QD), wetting layer states (WL), and bulk GaAs is labeled.

Based on our above observations, we have concluded that while the weakly confined InGaAs quantum dot or quantum well systems have the advantage of possessing optical transitions which are easier to access for QC experiments, the lack of excited quantum dot states may limit their use. As a result, we are also considering InAs quantum dot systems, in which the deeper confinement potential can allow for multiple excited state transitions. Figure 4 shows PL spectra obtained for high pumping intensity (allowing emission from excited states) for one such InAs quantum dot system. Three quantum dot transitions can be identified at energies below the wetting layer and bulk GaAs transitions. We are currently studying the influence of various

growth conditions on the excited state energy structure of the InAs quantum dots, in order to further tailor the system toward QC observations.

With the above characterization of the energy levels of the quantum dot systems, we are now preparing to perform optical experiments to study the QC effects of electromagnetically induced transparency (EIT) and slow light. These ultrafast pump-probe experiments will be performed in a waveguide geometry with pump and probe pulses co-propagating. Further refinements in the generation of the strong pump pulses and the detection of the weak probe pulses will be made. We will perform frequency resolved optical gating (FROG) on the transmitted probe pulses, both as a sensitive detection technique, and to allow for direct measurements of group velocity delays in slow-light experiments. These QC effects will be examined for a variety of level schemes in both the InGaAs and InAs systems discussed above.

The nonlinear measurements were delayed significantly by the lack of an optical parametric amplifier (OPA) to perform the high power pump probe spectroscopy that is believed to be the most successful experiment. The pump laser, a 1 kHz 800 nm, was available early in the effort, but the ability to dynamically scan the probe wavelength through the selected resonance was not purchased until half way through the LDRD. Even with the OPA, the 1 kHz repetition rate limits the experiments that can be performed due to the low signal to noise ratio.

4.1 Suggested Experiments for Observing Coherence Effects in SAQD

Several types of optical investigations would advance the goal of this LDRD and generate interesting science. These are summarized in order of their perceived importance for demonstrating QC effects.

Transient four-wave mixing (FWM) experiments through a waveguide were identified as the best way to observe QC effects, specifically EIT. Laser systems with high repetition rates

(70 to 80 MHz) with tunable delays between the pump and probe beams are needed to observe the coherent effects. The high repetition rate systems may not have the peak fluence needed, but intermediate systems to with repetition rates between 1 kHz and 80 MHz are available. Similar experiments would be spectral hole burning or Rabi oscillations [42, 43]. Rabi oscillations of the photocurrent has been demonstrated [44]. This could be extended to look at manipulations of the homogenous lifetime using electric fields [45]. FWM experiments sample the ensemble of SAQD. Alternatively, single SAQD could be measured if the appropriate confocal or near field microscope system were available [46, 47, 48]. Rabi oscillations have been observed using emission spectroscopy on single quantum dots [49,50]. For single quantum dots the inhomogeneous lifetime of the ensemble is not an issue and long homogeneous lifetimes, some approaching 1 nanosecond at liquid helium temperatures, have been reported for SAQD [51].

Carrier relaxation measurement in the near infrared using interband transitions are of interest to understand the time scales involved with populating carriers into different energy levels. This has been done using transient FWM, optically and electrically injected amplified spontaneous emission, differential transmission, and emission spectroscopy [52, 53, 54, 55, 56]. The carrier dynamics in SAQD is well understood, but it would be interesting to see how the present samples compare to proposed models of carrier relaxation. This work could be extended to look at coupled quantum dots (quantum molecules) [57]. The carrier dynamics of the intrasubband carriers have not been studied as thoroughly as the interband case. Several measurements have implied the existence of a phonon bottleneck under unipolar carrier conditions, but clear measurement of the phonon limited rate has not been performed.

The original proposal would use interband (conduction to valence band) transitions of the SAQD. This assumes that there is a one to one coupling of the electron and hole states of the

SAQD [58]. The alternative proposal is that there are many hole states and a smaller number of electron states that do not have one-to-one coupling [59]. While the experimental evidence for the former case is sound, this is an underlying assumption that should be assessed. Other energy levels might be accessed using the polarization of the different hole states of the semiconductor, similar to what was been done for quantum dots formed from interface fluctuations of thin GaAs/AlGaAs QW[50,60]. This could only be achieved using normal incidence geometry with multiple layer of SAQD to enhance the absorbance [61,62]. Intrasubband transitions (energy levels in the conduction band) could provide other combinations of energy levels that could be accessed. The ground state could be populated by doping the SAQD. These efforts could lead to demonstration of dark state spectroscopy with SAQD.

5.0 LDRD SUMMARY

Referred publications resulting from the work:

H.C. Schneider, W.W. Chow, S.W. Koch, "Excitation-induced dephasing in semiconductor quantum dots," Physical Review B, (2004), 70, 235308

W.W. Chow, H.C. Schneider, M.C. Phillips, "Theory of quantum-coherence phenomena in semiconductor quantum dots," Physical Review A, (2003), 68, 053802

H.C. Schneider, W.W. Chow, S.W. Koch, "Influence of coupling between localized and continuum states in InGaN quantum-dot systems," Physica Status Solidi B, (2003), 238, 589

W. W. Chow and S. W. Koch, 'Theory of semiconductor quantum-dot laser dynamics," IEEE Journ. Quantum Electron. **41**, 495-505, 2005

W.W. Chow and H.C. Schneider, "Theory of laser gain in InGaN quantum dots," Appl. Phys. Lett. **81,** 2566-2568, 2002

Y. Sun, S.F. Cheng, G. Chen, R.F. Hicks, J.G. Cederberg, R.M. Biefeld, "The effect of antimony in the growth of InAs quantum dots in GaAs (001)," Journal of Applied Physics, (2005), 97, 053503

J.G. Cederberg, F.H. Kaatz, R.M. Biefeld, "The impact of growth parameters on the formation of InAs quantum dots on GaAS(100) by MOCVD," Journal of Crystal Growth, (2004), 261, 197

J.G. Cederberg and S.R. Lee, "Technique to evaluate composition and strain in thin heterostructures," submitted to the Journal of Crystal Growth

J.G. Cederberg, "Segregation layer control of quantum dot formation during the growth of $In_{0.4}Ga_{0.6}As$ on GaAs(001) by metal-organic vapor phase epitaxy," submitted to the Journal of Applied Physics

All other reports and publications from the work: 1

Number of Patent Disclosures: 0

Number of Staff Hired: 0

Number of Applications: 0

Number of Post Docs: 2

Number of Patents: 0

Number of Students: 0

6.0 REFERENCES

1. P. Borri, W. Langbein, J. Mork, J.M. Hvam, F. Heinrichsdorff, M.-H. Mao, D. Bimberg, Phys. Rev. B., **60**, (1999), 7784.
2. P. Borri, W. Langbein, S. Schneider, U. Woggon, R.L. Sellin, D. Ouyang, D. Bimberg, Phys. Rev. Lett., **87**, (2001), 157401.
3. D. Birkedal, K. Leosson, J.M. Hvam, Phys. Rev. Lett., **87**, (2001), 227401.
4. D. Leonard, M. Krishnamurthy, C. M. Reaves, S. P. Denbaars, and P. M. Petroff, Appl. Phys. Lett., **63**, (1993), 3203.
5. D.J. Eaglesham, M. Cerrulo, Phys. Rev. Lett., **64**, (1990), 1943.
6. K. Kamath, P. Bhattachaya, J. Phillips, J. Crystal Growth, **175/176**, (1997), 720.
7. F. Heinrichsdorff,a) A. Krost, M. Grundmann, and D. Bimberg, A. Kosogovb) and P. Werner, Appl. Phys. Lett., **68**, (1996), 3284.
8. J.M. Moison, C. Guille, F. Houzay, F. Barthe, M. Van Rompany, Phys. Rev. B, **40**, (1989), 6149.
9. R. Kaspi, K.R. Evans, Appl. Phys. Lett., **67**, (1995), 819.
10. A. Ohtake, M. Ozeki, Phys. Rev. B., **65**, (2002), 155318.
11. H. Toyoshima, T. Niwa, J. Yamazaki, A. Okomoto, Appl. Phys. Lett., **63**, (1993), 821.
12. K. Muraki, S. Fukatsu, Y. Shiraki, R. Ito, Appl. Phys. Lett., **61**, (1992), 557.
13. J.M. Garcia, J.P. Silveira, F. Briones, **77**, (2000), 409.
14. D.J. Bottomley, Appl. Phys. Lett., **72**, (1998), 783.
15. J-M. Gerard, Appl. Phys. Lett., **61**, (1992), 2096.

16. R. Leon, C. Lobo, J. Zou, T. Romeo, D.J.H. Cockayne, Phys. Rev. Lett., **81**, (1998), 2486.
17. R. Leon, J. Wellman, X.Z. Liao, J. Zou, D.J.H. Cockayne, Appl. Phys. Lett., **76**, (2000), 1558.
18. X.G. Zhang, D.W. Parent, P. Li, A. Rodriguez, G. Zhao, J.E. Ayers, F.C. Jain, J. Vac. Sci. Tech., **18B**, (2000), 1375.
19. J.G. Cederberg, S.R. Lee, unpublished results.
20. J. Tersoff, F.K. LeGoues, Phys. Rev. Lett., **72**, (1994), 3570.
21. J. Tersoff, M.D. Johnson, B.G. Orr, Phys. Rev. Lett., **78**, (1997), 282.
22. A. Sasaki, E.R. Weber, Z. Liliental-Weber, S. Ruvimov, J. Washburn, Y. Nabetani, Thin Solid Films, **367**, (2000), 277.
23. B.W. Wessels, J. Vac. Sci. Tech., **B15**, (1997), 1056.
24. C.W. Snyder, B.G. Orr, H. Munekata, Appl. Phys. Lett., **62**, (1993), 46.
25. G.B. Arfken, H.-J. Weber, *Mathematical methods for physicists*, (San Diego: Academic Press, 2001), p. 952.
26. M. Berti, A.V. Drigo, G. Rossetto, G. Torzo, J. Vacuum Sci. Tech., **B15**, 1794, (1997).
27. D. Zhi, H. Davock, R. Murry, C. Roberts, T.S. Jones, D.W. Pashley, P.J. Goodhew, B.A. Joyce, J. Appl. Phys., **89**, 2079, (2001).
28. T.J. Krzyzewski, P.B. Joyce, G.R. Bell, T.S. Jones, Surface Sci., **517**, 8, (2002).
29. A.A. El-Emawy, S. Birudavolu, P.S. Wong, Y.-B. Jiang, H. Xu, S. Huang, D.L Huffaker, J. Appl. Phys., **93**, 3529, (2003).

30. A.E. Zhukov, V.M. Ustinov, A.R. Kovsh, A. Yu. Egorov, N.A. Maleev, N.N. Ledentsov, A.F. Tsatsul'nikov, M.V. Maximov, Yu.G. Musikhin, N.A. Bert, P.S. Kop'ev, D. Bimberg, Zh.I. Alferov, Semiconductor Sci. Tech., **14**, 575, (1999).
31. H.Y. Liu, X.D. Wang, B. Xu, D. Ding, W.H. Jiang, J. Wu, Z.G. Wang, J. Crystal Growth, **213**, 193, (2000).
32. A. Passaseo, G. Maruccio, M. De Vittorio, R. Rinaldi, R. Cingolani, M. Lomascolo, Appl. Phys. Lett., **78**, 1382, (2001).
33. O. Suekane, S. Hasegawa, M. Takata, T. Okui, H. Nakashima, Material Sci. Engr., **B88**, 158, (2002).
34. K. Tillmann, D. Gerthsen, P. Pfundstein, A. Forster, K. Urban, J. Appl. Phys., **78**, 3824, (1995).
35. J. Johansson, W. Seifert, J. Crystal Growth, **234**, 139, (2002).
36. J. Johansson, W. Seifert, J. Crystal Growth, **234**, 132, (2002).
37. P.B. Joyce, T.J. Krzyzewski, G.R. Bell, T.S. Jones, S. Malik, D. Childs, R. Murray, **227-228**, 1000, (2001).
38. K. Shiramine, T. Itoh, S. Muto, T. Kozaki, S. Sato, J. Crystal Growth, **242**, 332, (2002).
39. Y. Nakata, K. Mukai, M. Sugawara, K. Ohtsubo, H. Ishikawa, N. Yokoyama, J. Crystal Growth, **208**, 93, (2000).
40. B.J. Riel, K. Hinzer, S. Moisa, J. Fraser, P. Finnie, P. Piercy, S. Farfard, Z.R. Wasilewski, J. Crystal Growth, **236**, 145, (2002).
41. A. Yamashiki, T. Nishinaga, J. Crystal Growth, **198/199**, 1125, (1999).

42. P. Borri, W. Langbein, S. Schneider, U. Woggon, R.L. Sellin, D. Ouyang, D. Bimberg, Phys. Rev. B., **66**, (2002), 081306-1.

43. H. Nakamura, S. Nishikawa, S. Kohmoto, K. Kanamoto, K. Asakawa, J. Appl. Phys., **94**, (2003), 1184.

44. A. Zrenner, E. Beham, S. Stufler, F. Findeis, M. Bichler, G. Abstreiter, Nature, **418**, (2002), 612.

45. R. Oulton, J.J. Finley, A.D. Ashmore, I.S. Gregory, D.J. Mowbray, M.S. Skolnick, M.J. Steer, S.-L. Liew, M.A. Migliorato, A.J. Cullis, Phys. Rev. B., **66**, (2002), 045313.

46. T. Matsumoto, M. Ohtsu, K. Matsuda, T. Saiki, H. Saito, K. Nishi, Appl. Phys. Lett., **75**, (1999), 3246.

47. T. Guenther, C. Lienau, T. Elsaesser, M. Glanemann, V. M. Axt, T. Kuhn. S. Eshlaghi, A.D. Wieck, Phys. Rev. Lett., **89**, (2002), 057402-1.

48. A. Högele, M. Kroner, S. Seidl, K. Karrai, M. Atatüre, J. Dreiser, A. Imamoğlu, R.J. Warburton, A. Badolato, B.D. Gerardot, P.M. Petroff,. Appl. Phys. Lett., **86**, (2005), 221905.

49. H. Kamada, H. Gotoh, J. Temmyo, T. Takagahara, H. Ando, Phys. Rev. Lett., **87**, (2001), 246401-1.

50. N.H. Bonadeo, J. Erland, D. Gammon, D. Park, D.S. Katzer, D.G. Steel, Science, **282**, (1998), 1473.

51. M. Bayer, A. Forchel, Phys. Rev. B, **65**, (2002), 041308-1

52. P. Borri, W. Langbein, J.M. Hvam, F. Heinrichsdorff, M.-H. Mao, D. Bimberg, J. Appl. Phys., **89**, (2001), 6542.

53. C. Lingk, G. von Plessen, J. Feldmann, K. Stock, M. Arzberger, G. Böhm, M.-C.Amann, G. Abstreiter, Appl. Phys. Lett., **76**, (2000), 3507.

54. P. Borri, W. Langbein, J.M. Hvam, F. Heinrichsdorff, M.-H. Mao, D. Bimberg, Appl. Phys. Lett. **76**, (2000), 1380.

55. T. S. Sosnowski, T.B. Norris, H. Jiang, J. Singh, K. Kamath, P. Bhattacharya, Phys. Rev. B, **57**, (1998), R9423.

56. B. Ohnesorge, M. Albrecht, J. Oshinowo, A. Forchel, **54**, (1996), 11532.

57. J. Urayama, T.B. Norris, B. Kochman, J. Singh, P. Bhattacharya, Appl. Phys. Lett., **76**, (2000), 2394.

58. I.E. Itskevich, M.S. Skolnick, D.J. Mowbay, I.A. Trojan, S.G. Lyapin, L.R. Wilson, M.J. Steer, M. Hopkinson, L. Eaves, P.C. Main, Phys. Rev. B, **60**, (1999), R2185.

59. M. Grundmann, N.N. Ledentsov, O. Stier, J. Bohrer, D. Bimberg, V.M. Ustinov, P.S. Kopev, Z.I. Alferov, Phys. Rev. B, **53** (1996) 10509

60. T.H. Stievater, X. Li, T. Cubel, D.G. Steel, D. Gammon, D.S. Katzer, D. Park, Appl. Phys. Lett., **81**, (2002), 4251.

61. M. Pailard, X. Marie, P. Renucci, T. Amand, A. Jbeli, J.M. Gerard, Phys. Rev. Lett., **86**, (2001), 1634.

62. A.S. Lenihan, M.V. Gurudev Dutt, D.G. Steel, S. Ghosh, P.K. Bhattacharya, Phys. Rev. Lett., **88**, (2002), 223601-1

DISTRIBUTION

1	MS1427	J.M. Phillips	1100
1	MS1056	B.L. Doyle	1110
1	MS1415	D.E. Peebles	1112
1	MS1415	N.A. Modine	1112
1	MS1415	C. Gutierrez	1114
1	MS1415	J.A. Floro	1114
1	MS1415	J.C. Barbour	1120
1	MS0601	D.L. Barton	1123
1	MS0601	W.W. Chow	1123
1	MS1415	M. Lee	1123
1	MS0601	S.R. Lee	1123
1	MS1415	M.P. Lilly	1123
1	MS1415	S.K. Lyo	1123
1	MS0601	W. Pan	1123
1	MS1415	E.A. Shaner	1123
1	MS0601	R. M. Biefeld	1126
4	MS0601	J.G. Cederberg	1126
1	MS0601	M.E. Coltrin	1126
1	MS0601	D.P. Nelson	1126
1	MS1423	G.A. Hebner	1128
1	MS1421	J.A. Simmons	1130
1	MS1413	N.D. Shinn	1131
1	MS0603	M.C. Wanke	1713
1	MS0603	G.M. Peake	1742
1	MS0986	W.J. Zubrzcki	2666
2	MS9018	Central Technical Files	8945-1
2	MS0899	Technical Library	4536
1	MS0123	D. Chavez, LDRD Office	01011